



Moving mass over a viscoelastic system: asymptotic behaviours and insights into nonlinear dynamics

M. Argenziano · A. Cutolo · E. Babilio ·
A. R. Carotenuto · M. Fraldi

Received: 30 September 2022 / Accepted: 6 April 2023
© The Author(s) 2023

Abstract Moving masses are of interest in many applications of structural dynamics, soliciting in the last decades a vast debate in the scientific literature. However, despite the attention devoted to the subject, to the best of the authors' knowledge, there is a lack of analysis about the fate of a movable mass when it rolls or slips with friction on a structure. With the aim of elucidating the dynamics of the simplest paradigm of this system and to investigate its asymptotic response, we make reference to a two-degree-of-freedom model made of an elastically vibrating carriage surmounted by a spherical mass, facing the problem both theoretically and experimentally. In case of linear systems, the analytical solutions and the laboratory tests performed on *ad hoc* constructed prototypes highlighted a counterintuitive asymptotic dynamics, here called *binary*: in the absence of friction at the interface of the bodies' system, the mass holds its initial position or, if nonzero damping acts, at the end of the motion it is in a position that exactly recovers the initial relative distance carriage–sphere. While the first result might be somewhat obvious, the second appears rather surprising. Such a binary behaviour is also confirmed for a Duffing-

like system, equipped with cubic springs, while it can be lost when non-smooth friction phenomena occur, as well as in the case of elastic springs restraining the motion of the sphere. The obtained analytical results and the numerical findings, also confirmed by experimental evidences, contribute to the basic understanding of the role played by the damping parameters governing the systems' dynamics with respect to its asymptotic behaviour and could pave the way for designing active or passive vibration controllers of interest in engineering.

Keywords 2-DOF systems · Moving mass · Nonlinear dynamics · Non-smooth friction · Duffing model

1 Introduction

Problems of dynamic actions that vary with position play a crucial role in several applications of structural dynamics and have been widely investigated in the literature for many decades [1–10]. The seminal book by Frýba [11] analyses the effects of moving loads on solids and structures, as strings, rigid-plastic beams, thin-walled beams and beams on elastic foundations, frames and arches, plates and elastic spaces. Such problems are typically studied in transportation engineering since structures, as bridges, railways and roadways, are subjected to moving loads often generated by vehicles, which move with constant or variable speeds along the structure and produce inertial effects due to their

M. Argenziano · A. Cutolo · E. Babilio · A. R. Carotenuto ·
M. Fraldi (✉)
Department of Structures for Engineering and Architecture, University of Naples "Federico II", Naples, Italy
e-mail: fraldi@unina.it

M. Argenziano
Department of Engineering, University of Palermo, Palermo, Italy

masses and trajectories. In addition, the speed of the vehicles and the flexibility of the main structure are of great importance due to dynamic interaction phenomena. Indeed, an accurate estimation of such loads is required and mandatory for a reliable design, since a structure subjected to moving loads exhibits deflection and stresses significantly higher than in the static case. However, the problem is not strictly confined to transportation engineering, being relevant to structures of interest to the everyday life, as parking garages and aircraft carriers, high-speed precision machining, magnetic disc drives and cables transporting materials, to name a few. The moving loads, where their inertial effects should be taken into account, are more precisely called moving masses [12]. In fact, as illustrated by Ting et al. [13], when the velocity of the sliding mass is not relatively small, a coupling between the two bodies occurs and the inertial effects cannot be referred to the two structural parts as standalone.

In facing planar moving load problems, both the directions of the load and its velocity are quite often assumed as relevant, thus leading to a bidirectional dynamics, where the interaction between the load and the deformability of the supporting body assumes a paramount importance. In this perspective, several papers [14–19] analyse the effect of a mass moving along a flexible Euler–Bernoulli supported beam, focusing on the influence of the mass ratio and the bending rigidity of the beam on the dynamic response of the overall system. Lee and Kim [20] provide an analytical and numerical method for getting a response of an elastically simply supported Timoshenko beam to a moving load. Considering the problem of the motion of a sphere on a flexible cable, Aristoff et al. [21], by combining experimental and theoretical investigations, demonstrate that the time taken by a sphere for descending along an elastic beam, the so-called *elastochrone*, exceeds that from the classical brachistochrone.

All the above-mentioned works assume that deformations and deflections remain small. To overcome this limitation, an upgrade of moving mass problems is provided by Zhao et al. [22], who develop a theory for large deformations based on Cosserat rod theory for studying the dynamics of mass-cable systems. The problems of taut strings carrying a movable mass [23] or travelled by a train of forces [24] are also addressed in the literature. Also, the noteworthy paradox of the discontinuity in the trajectory close to the end support exhibited by the solution of string vibration under a moving mass

has attracted attention [25]. In [26] the problem is studied through a kinematically exact nonlinear model, in which the motion of the point mass in the direction of the string in the reference configuration, say horizontal direction, is firstly considered unknown, while a driving force is assigned in the same direction. By assuming that the dynamic tension and the mass of the string are negligible, the existence of a horizontal reactive force at the mass–string contact, preventing the mass to reach the right support, is highlighted. Further upgrades of the mentioned study are introduced in [27,28].

In addition to the dynamic modelling and the response analysis of beams and strings subjected to a moving mass/load, the vibration control of these structures is another important issue that has received great attention [29–33]: several control algorithms have been proposed to suppress the vibration of the beam thanks to the inertial and dissipative effects induced by the moving mass sliding on the support. The inertial and dynamic effects derived by the motion of an added solid mass are also becoming of increasing interest in the field of fluid mechanics [34–36].

Several papers focus on moving loads problems characterised by unidirectional dynamics, where the load/mass does not interact with the deformability of the supporting structures, which can be assumed as rigid. In particular, there is growing interest in devices that can actively or passively control the dynamics of bodies: a carried mass moving on a rigid track may be used to reduce its dynamic amplification, as in the case of tuned mass dampers [37,38], or the motion of a mass inside rigid boxes can excite the locomotion of the overall system, as in the case of capsule robots [39–41].

However, although so many moving masses/loads problems have been in-depth investigated, with different purposes and applications and by adopting increasingly refined models, to the best of the author’s knowledge, no research paper focuses on the asymptotic behaviour of the simplest “toy system” case of an elastically vibrating rigid support with a mass free to move on it. To fill this gap, this paper deals with the dynamics of such a paradigmatic two degree-of-freedom (2-DOF) system, which allows predicting two different asymptotic responses of the mass. In the absence of friction at the interface between the carriage and the mass, the latter holds its initial position. If nonzero damping acts, at the end of the motion the mass is in a position that exactly recovers the initial relative distance carriage–

sphere. This behaviour, which we call *binary*, has been found analytically in Sect. 2.1, and also experimentally reproduced, through an *ad hoc* designed ad 3D printed set-up, for the first time in Sect. 2.2. Then, the effects of some nonlinearities on the binary asymptotic behaviour are discussed in Sect. 3 by considering either Duffing [42–45] or dry friction [46–48] terms. A further example is conceived by connecting the carriage to the moving mass through nonlinear elastic springs allowing tunable, pre-stretch induced stiffness in Sect. 4. Then some conclusions are reported in Sect. 5.

2 Binary dynamics of the simplest “toy system”: analytical and experimental results

2.1 Analytical solution for the linearly elastic system with moving mass

Let us consider a spherical mass moving on a sliding carriage, as shown in Fig. 1. In the hypothesis of small oscillations, the equations of the free vibration along the x direction are

$$m_1 \ddot{x}_1(t) + d \dot{x}_1(t) + k_1 x_1(t) - c(\dot{x}_2(t) - \dot{x}_1(t)) = 0, \tag{1}$$

$$m_2 \ddot{x}_2(t) + c(\dot{x}_2(t) - \dot{x}_1(t)) = 0, \tag{2}$$

where $x_i, \dot{x}_i, \ddot{x}_i$ $i = \{1, 2\}$ stand for displacement, velocity, acceleration, of carriage ($i = 1$) or sphere ($i = 2$) where the superimposed dot denotes the derivative with respect to time t . The masses of carriage and sphere are m_1 and m_2 , respectively; k_1 indicates the overall axial stiffness of the two springs anchored to the carriage; c and d are damping parameters.

We emphasise that, in the first step, we assume that the dissipation-inducing terms, as dynamic friction at the interface between the spherical mass and the carriage or between the carriage wheels and the substrate, the air drag forces on the sphere and carriage and the damping induced by synergistic effects of air trapped into the helical springs and internal damping, and so on, are all represented as effective linear viscous damping. However, the orders of magnitude of the terms incorporated in the damping parameters can be significantly different. For instance, for a spherical steel mass moving with velocity v and having diameter $\phi = 0.03$ m, the air drag force, typically evaluated as

$3\pi\mu_a v\phi$, with μ_a the air viscosity, is about 6 orders of magnitude lower than the rolling friction force, calculated as $2m_2g\mu_s/\phi$, being g acceleration of gravity and μ_d the dynamic friction coefficient, at the contact surface between the sphere and the vibrating carriage. These findings have been experimentally confirmed by *ad hoc* laboratory tests, which also allowed measuring the involved key parameters (see Sect. 2.2).

By setting $y_1(t) = \dot{x}_1(t)$ and $y_2(t) = \dot{x}_2(t)$, Eqs. (1)–(2) can be conveniently rearranged in matrix form as

$$\begin{pmatrix} \dot{x}_1 \\ \dot{x}_2 \\ \dot{y}_1 \\ \dot{y}_2 \end{pmatrix} = \begin{pmatrix} 0 & 0 & 1 & 0 \\ 0 & 0 & 0 & 1 \\ -k_1 m_1^{-1} & 0 & -(c+d)m_1^{-1} & c m_1^{-1} \\ 0 & 0 & c m_2^{-1} & -c m_2^{-1} \end{pmatrix} \begin{pmatrix} x_1 \\ x_2 \\ y_1 \\ y_2 \end{pmatrix}, \tag{3}$$

admitting the characteristic equation

$$\eta \left(m_1 m_2 \eta^3 + \left(d m_2 + c (m_1 + m_2) \right) \eta^2 + (c d + k_1 m_2) \eta + k_1 c \right) = 0, \tag{4}$$

where, for ease of notation, the time dependence is implied.

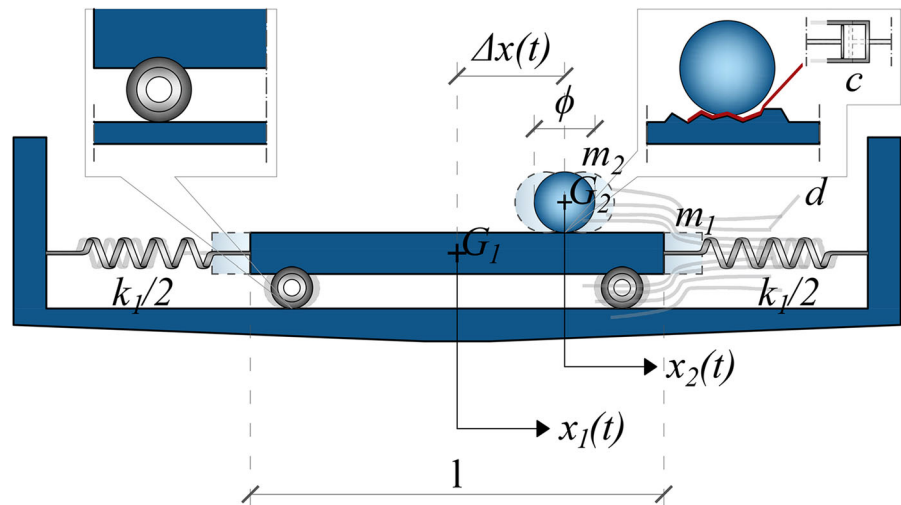
Since Eq. (4) has a vanishing root, among the other three ones, at least one is real. Therefore, eigenvalues can be written in closed form by using Cardano’s solution [49]. For the range of parameters of interest, each eigenvalue has an algebraic multiplicity equal to 1, and the problem is diagonalisable and characterised by a complete system of 4 eigenvectors. The general integral of the system, namely the vector $\mathbf{y}(t) \equiv (x_1(t), x_2(t), y_1(t), y_2(t))^T$, takes the form

$$\mathbf{y} = c_1 \mathbf{v}_1 + c_2 \mathbf{v}_2 e^{\eta_2 t} + c_3 \mathbf{v}_3 e^{\eta_3 t} + c_4 \mathbf{v}_4 e^{\eta_4 t}, \tag{5}$$

where $\mathbf{v}_i, i = \{1, \dots, 4\}$, are the eigenvectors associated to the eigenvalues η_i , and c_i represent the constants of integration to be determined by imposing the initial conditions. Explicit expressions of eigenvalues and eigenvectors of Eq. (3) are reported in “Appendix A”.

To capture the key features of the response of the system as the parameters vary, we exploit the analytical solution and perform a sensitivity analysis through six representative examples (see Fig. 2), in which the parameters take nonnegative values and the initial conditions, with $\Delta x(0)$ the initial distance between the cen-

Fig. 1 2-DOF model of a spherical mass moving on a sliding carriage



tres of gravity of carriage and sphere, are set as

$$\begin{aligned} x_1(0) &= 0.01 \text{ m}, \\ x_2(0) &= x_1(0) + \Delta x(0) = 0.03 \text{ m}, \\ \dot{x}_1(0) &= \dot{x}_2(0) = 0 \text{ m s}^{-1}. \end{aligned} \quad (6)$$

In Example A, $m_1 < m_2$ and $c = d < d_{\text{crit}}$, being $d_{\text{crit}} = 2\sqrt{m_1 k_1}$ the critical damping, thus leading to both the degrees of freedom showing harmonic damped responses (Fig. 2A).

In Example B, $m_1 < m_2$, $c < d$ and $d > d_{\text{crit}}$, and the response has overdamped behaviour on both the degrees of freedom (Fig. 2B).

More interestingly, Example C, where $m_1 < m_2$ and $c > d = 0$, i.e. damping on the carriage is negligible, while mutual damping is present, both responses x_1 and x_2 are damped. By virtue of Eq. (2), we can substitute the term $-c(\dot{x}_2 - \dot{x}_1)$ with $m_2 \ddot{x}_2$ in Eq. (1), thus attaining $m_1 \ddot{x}_1 + k_1 x_1 = -m_2 \ddot{x}_2$, which, if compared with graphs shown in Fig. 2C, allows recognising that the force $-m_2 \ddot{x}_2$ actually drives x_1 towards its rest position. This example shows that the moving mass exerts a damping action on the motion of the carriage. Despite an indirect damping is imparted on the carriage, the system in this case is different from classical tuned mass dampers, where typically the secondary mass is attached to the primary one through elastic constraints, modelled as springs [50]. Therefore, this system could represent the paradigm of a viscous tuned mass damper and it could pave the way for designing devices for the vibration control of interest in engineering.

Example D emphasises the damping role of a carried mass much larger than that of the carriage. Here,

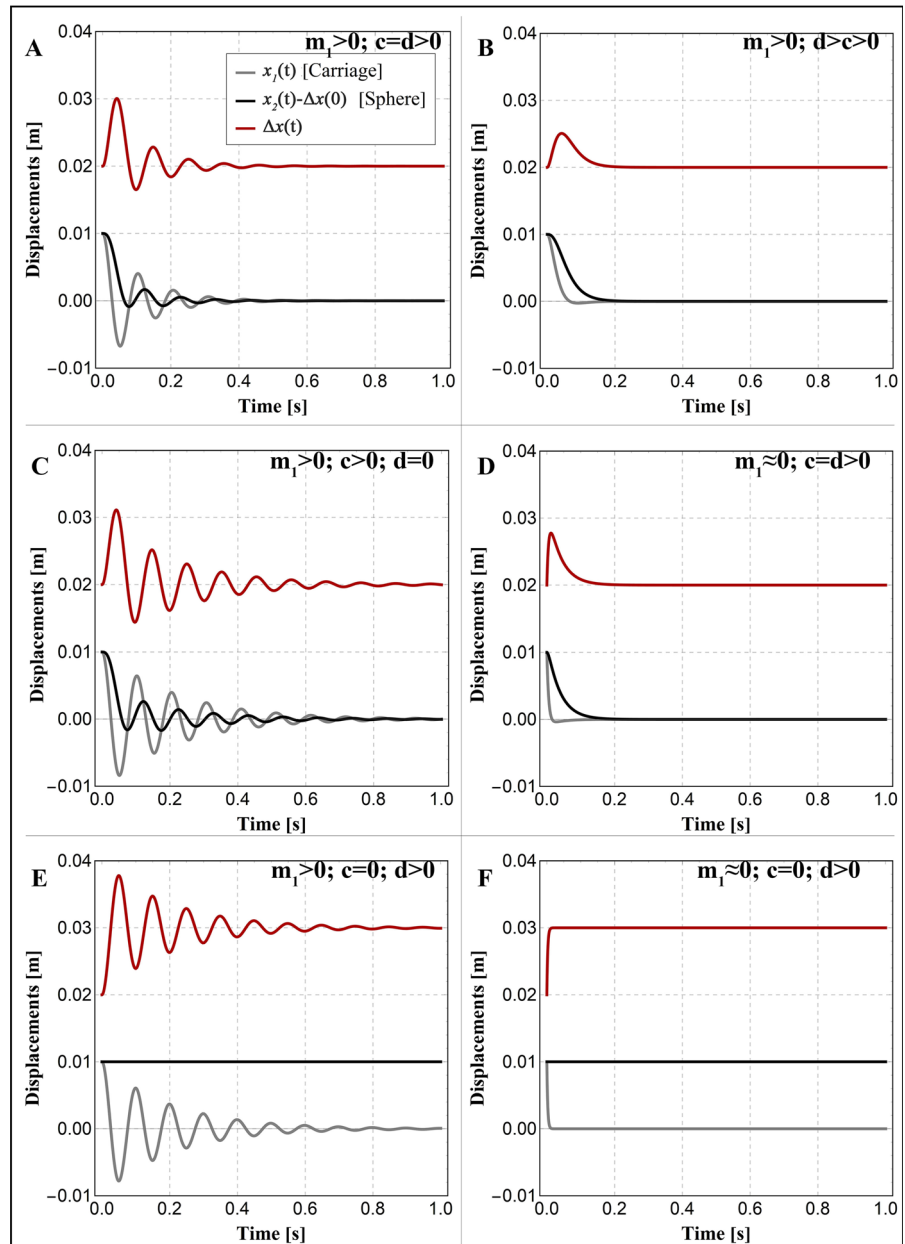
$m_1 \approx 0$ and $c = d < d_{\text{crit}}$ lead to a response towards resting position without oscillation. Notice that to avoid division by zero, m_1 must be not null in Eq. (3), so that $m_1 \approx 0$ in performed test stands for $m_1 = 10^{-80}$ kg.

Furthermore, the most intriguing feature of responses, from A to D, as shown in Fig. 2, is that while the displacement x_1 (grey line) of the carriage invariably asymptotically approaches to 0, the displacement x_2 of the sphere goes to $\Delta x(0)$. Indeed, chosen any reference point on the carriage, whatever is the initial displacement $x_1(0)$, the sphere, after the transient phase, reaches its rest position whose relative distance from the reference point will be equal to the initial relative distance $\Delta x(0)$, as if it remembered where it was at the beginning.

We highlight that this interesting behaviour, computed in closed form by solving Eqs. (1)–(2) complemented with the initial conditions given by Eq. (6), is somehow unexpected and, to the best of authors' knowledge, not reported in the scientific literature.

This behaviour changes abruptly for $c = 0$, c actually playing both the role of the coupling parameter between Eqs. (1)–(2) and that of a bifurcation parameter. Indeed, for $c = 0$, no interaction between the two bodies occurs and, for the initial conditions reported in Eq. (6), the sphere rests for any t , which is an obvious consequence of the fact that, in such a case, $x_2(t) = x_2(0) + \dot{x}_2(0)t = 0.03 \text{ m}$. In addition, we also emphasise that such a behaviour of the sphere is expected by physical intuition, that is even before observing that Eqs. (1)–(2) become mathematically uncoupled for $c = 0$.

Fig. 2 Sensitivity analysis of the system made up of a spherical mass moving on a sliding carriage. In all graphics, but when null, the following parameters are assumed: $m_1 = 0.10$ kg, $m_2 = 0.04$ kg, $k_1 = 400$ N m⁻¹, $c = 1$ N s m⁻¹, and $d = 1$ or 10 N s m⁻¹



It is also interesting to observe that one expects two different behaviours also in case of two harmonic oscillators which are equal to each other but for the damping, being one damped and the other undamped. Indeed, the former system is structurally stable, while the latter not. In fact, in the case of the undamped harmonic oscillator, the action of any arbitrarily small damping force changes the qualitative behaviour of the solutions from that of a centre to a focus at the origin [51]. However,

we emphasise that here the situation is different, or at least apparently less well documented. In fact, Eqs. (1)–(2) present two independent parameters of damping, namely c and d , being only the former responsible for the behaviour we shall henceforth call *binary*. To recognise this, one can compare results from Examples A to D to those from two further ones (Fig. 2E and F), both characterised by $c = 0$ and $d > 0$, chosen as representative of the second asymptotic behaviour

of the sphere. In both cases, the sphere does not have any motion, resting in its initial position, while the carriage exhibits a damped motion, due to $d > 0$, with or without oscillations (respectively, underdamped for $m_1 > 0$, or overdamped for $m_1 \approx 0$).

Figure 3A and C shows the phase trajectories of carriage and Fig. 3B and D those of the sphere for the two cases shown in Fig. 2E ($c = 0$) and Fig. 2A ($c > 0$), emphasising the binary asymptotic behaviour and the counterintuitive response for $c > 0$.

2.2 Experimental confirmation of the binary behaviour: 3D prototype and laboratory tests

With the aim of providing experimental validations of the analytical results, a prototype of the analysed model has been designed with the aid of the 3D CAD/CAM software Solid Edge [52] (see Fig. 4A and C) and then manufactured using Thermoplastic Polyurethane (TPU 92A) on the STRATASYS F170 3D printer.

In order to have the ability to adjust the inclination of the wheeled, main carriage (the blue-coloured element in Fig. 4B, C and D) and keep it horizontal, two supports have been 3D printed (black-coloured in Fig. 4B, C and D) and equipped with regulating bolts.

An aluminium rail surmounts the carriage to force the secondary mass into a perfectly unidirectional motion.

The carriage is connected to external clamps through pre-stretched elastic springs, as shown in Fig. 4B and D. The spring elasticity has been estimated through uniaxial tests performed on many specimens by means of the ElectroForce[®] 200N 4 Motor Planar Biaxial TestBench machine (Fig. 4E). Because of pre-stretch, depending on the displacement of the carriage, a non-linear response could be expected. However, in the small-on-large hypothesis, the linearity can still be retained, and the equivalent, effective stiffness is the mean value of those registered in the range of several pre-stretch values. From experimental evidence,

Fig. 3 Phase space plots for the carriage (top panels) and the sphere (bottom panels), by assuming $x_1(0) = 0.01$ m and $x_2(0) = x_1(0) + \Delta x(0) = 0.03$ m, $m_1 = 0.10$ kg, $m_2 = 0.04$ kg, $k_1 = 400$ N m⁻¹, and $d = 1$ N s m⁻¹. The damping parameter takes values $c = 0$ N s m⁻¹ (left column panels) or $c = 1$ N s m⁻¹ (right column panels)

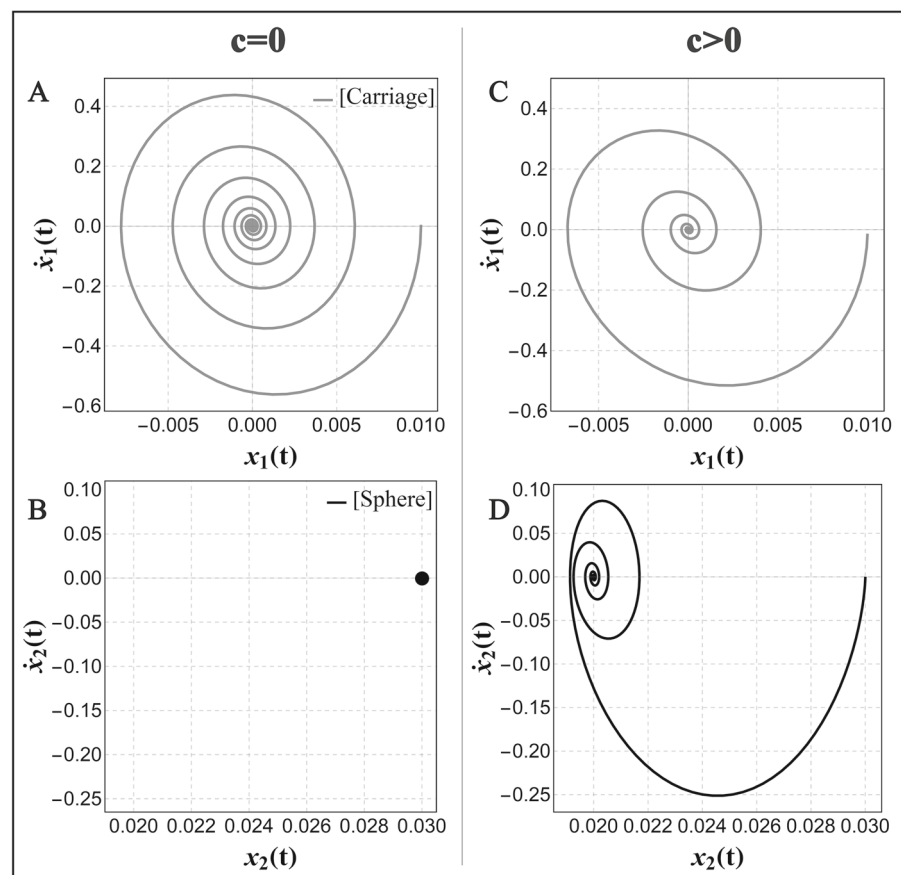
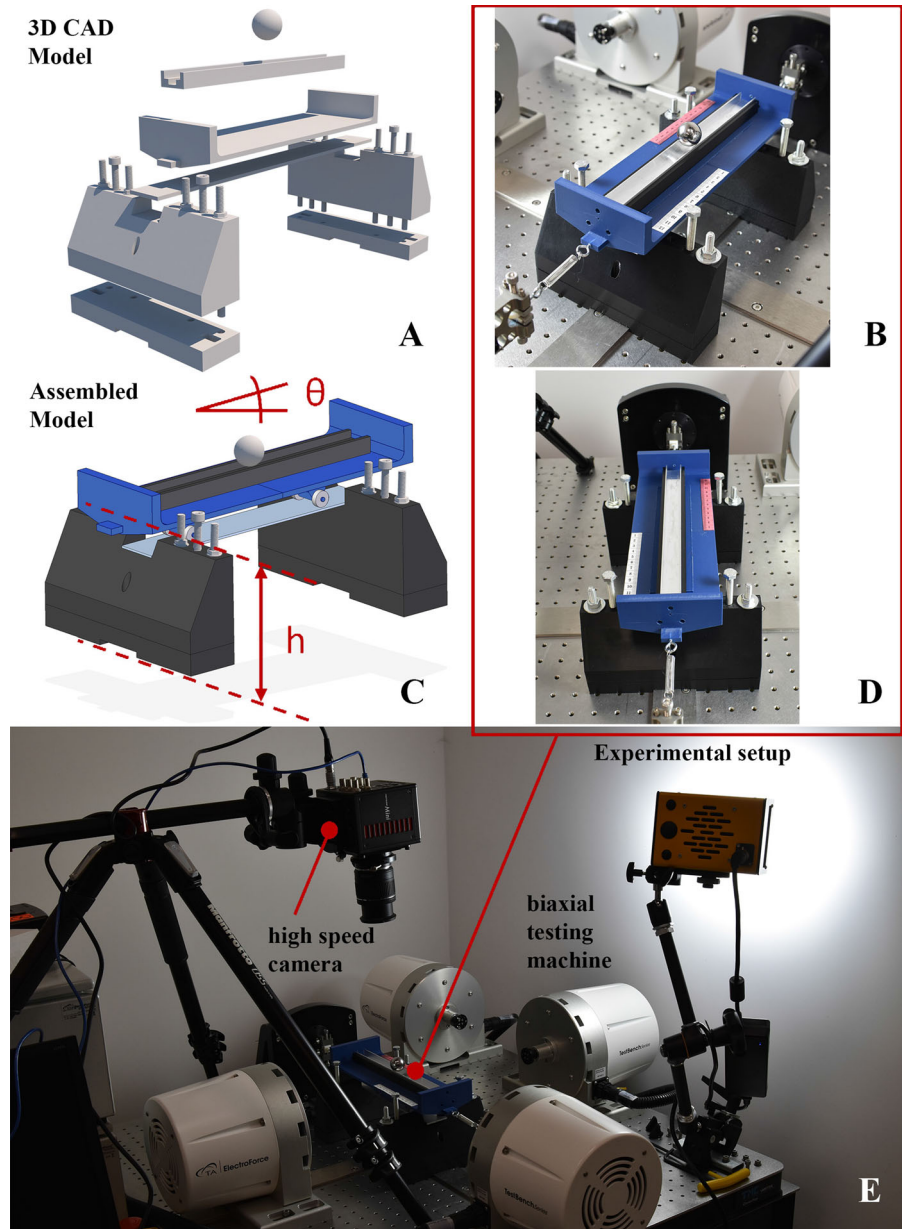


Fig. 4 3D CAD model of the laboratory set-up system (A and C); 3D printed prototype of the model (B and D); experimental set-up (E)



the tangent modulus of the springs varies in the order of tens N m^{-1} .

The primary mass to be considered is a compound of the masses of the carriage, wheels, rail, and elastic restraints and is measured as 0.478 kg, by using a precision scale. For the secondary mass, several steel spheres, from 0.067 kg to 0.288 kg, have been utilised to have the possibility of reproducing either low mass ratio cases up to mass ratios greater than 0.5.

A high-speed Photron's camera CMOS MINI FAST-CAM AX100 (Fig. 4E) has been placed over the system to record displacements at a sampling rate of 4000 fps at image resolution of 1024×1024 pixels.

By focusing on the free mass case, in order to grasp the binary behaviour provided by the analytical predictions of Sect. 2.1, two different experimental set-ups are organised: (i) the aluminium rail and the sphere have been oiled with the aim of nullifying the friction in the sphere–carriage interface and of reproducing the

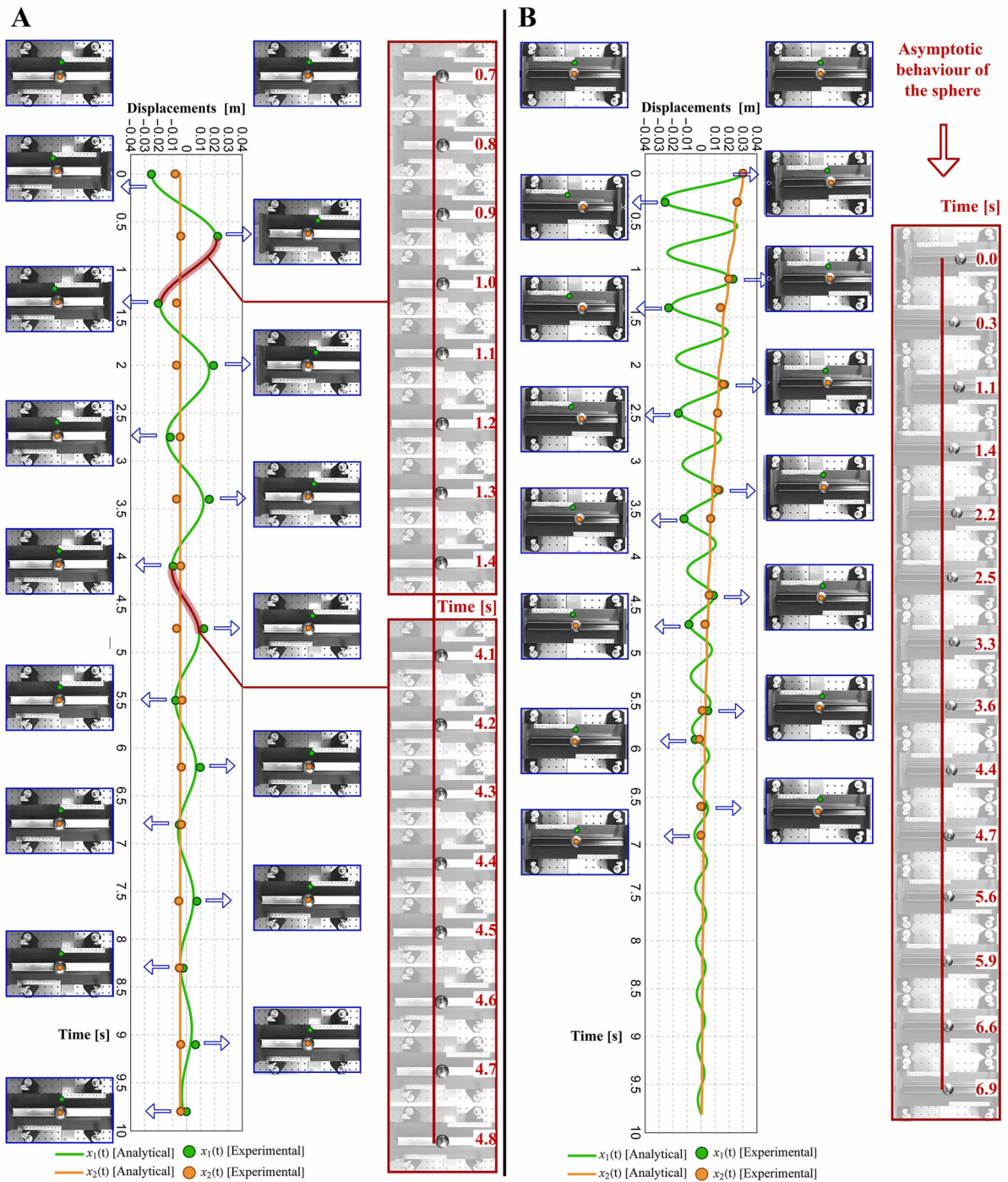


Fig. 5 Experimental validation of the asymptotic binary behaviour for the free mass example, with parameters measured or derived from experimental calibration: $m_1 = 0.478$ kg,

$m_2 = 0.152$ kg, $d = 0.2$ N s m^{-1} , $k_1 = 10$ N m^{-1} , and c nullified by oiling (case A) or $c = 0.06$ N s m^{-1} (case B)

cases E and F of Fig. 2 (Fig. 5A); (ii) a TPU layer is mounted over the aluminium rail for increasing the friction between the sphere and the primary mass, thus replicating the non zero friction case (Fig. 5B). While the stiffness and mass parameters are experimentally measured, the damping coefficients c and d are calculated through curve-fitting aimed at converging the experimental results with the theoretical curves.

In case A, the initial distance between the centres of gravity of the carriage and the sphere is set as $\Delta x(0) = 0.021$ m. For activating dynamics of the system, the carriage is initially displaced of 0.025 m in the opposite direction to $\Delta x(0)$ (i.e. $x_1(0) = -0.025$ m) and then released. From Fig. 5A, it can be seen that the theoretical curves, in terms of the time histories of displacement of the two masses, perfectly match the experimental points, confirming that no dynamic interaction occurs between the sphere and the carriage in the case of zero friction, with the sphere remaining at rest.

In case B, an initial step displacement $x_1(0) = 0.03$ m is imposed on the carriage, while the centres of gravity of sphere and carriage are vertically aligned, $\Delta x(0) = 0.00$ m. From Fig. 5B, it can be observed that, with friction at the interface, the sphere actually returns to its initial relative position, i.e. x_2 approaches $\Delta x(0)$, in excellent agreement with the analytical time history.

As already stated, several springs with different stiffness and spheres with different diameters, to represent cases with low, intermediate and high mass ratios, have been considered, while keeping invariant the primary mass. Invariably, tests showed the sphere achieving a rest position equal to the initial relative position between its centre of gravity and that of the carriage.

3 Effects of nonlinearities on the asymptotic behaviour of the system

In Sect. 2, the binary asymptotic behaviour of the system has been first analytically found and then confirmed through experimental validation. As above mentioned, by considering a linear system, this behaviour depends essentially on the parameter c .

In the following, to investigate the effects of nonlinearities on the dynamics of the system, especially with reference to the asymptotic behaviours, we consider

two nonlinear models, the first equipped with nonlinear stiffness and the second with nonlinear damping.

The nonlinear differential equations will be integrated, for given initial conditions and over assigned time intervals from t_{\min} to t_{\max} , using the general numerical differential equation solver `NDSolve` available in *Mathematica*[®] [53]. `NDSolve` has many different built-in methods for computing solutions and, by default, `NDSolve` automatically chooses the possibly most appropriate method for the differential equations under integration. Furthermore, during the integration process one method can call another, if needed.

The solution is found iteratively, starting at a particular value of the independent variable, and then taking a sequence of steps, trying eventually to cover the whole range t_{\min} to t_{\max} . `NDSolve` uses an adaptive procedure to determine the size of the steps, which is made smaller and smaller until the solution reached satisfies either the value of the chosen accuracy or precision, through error estimates. For a wide description of methods and available options for their settings, as well as of the control mechanisms set up for writing new user-defined numerical integration algorithms to be used as specifications for `NDSolve`, we refer to [54].

3.1 Duffing-like stiffness

We consider the elastic restraints as nonlinear and write the equations of motion of the system shown in Fig. 1 as

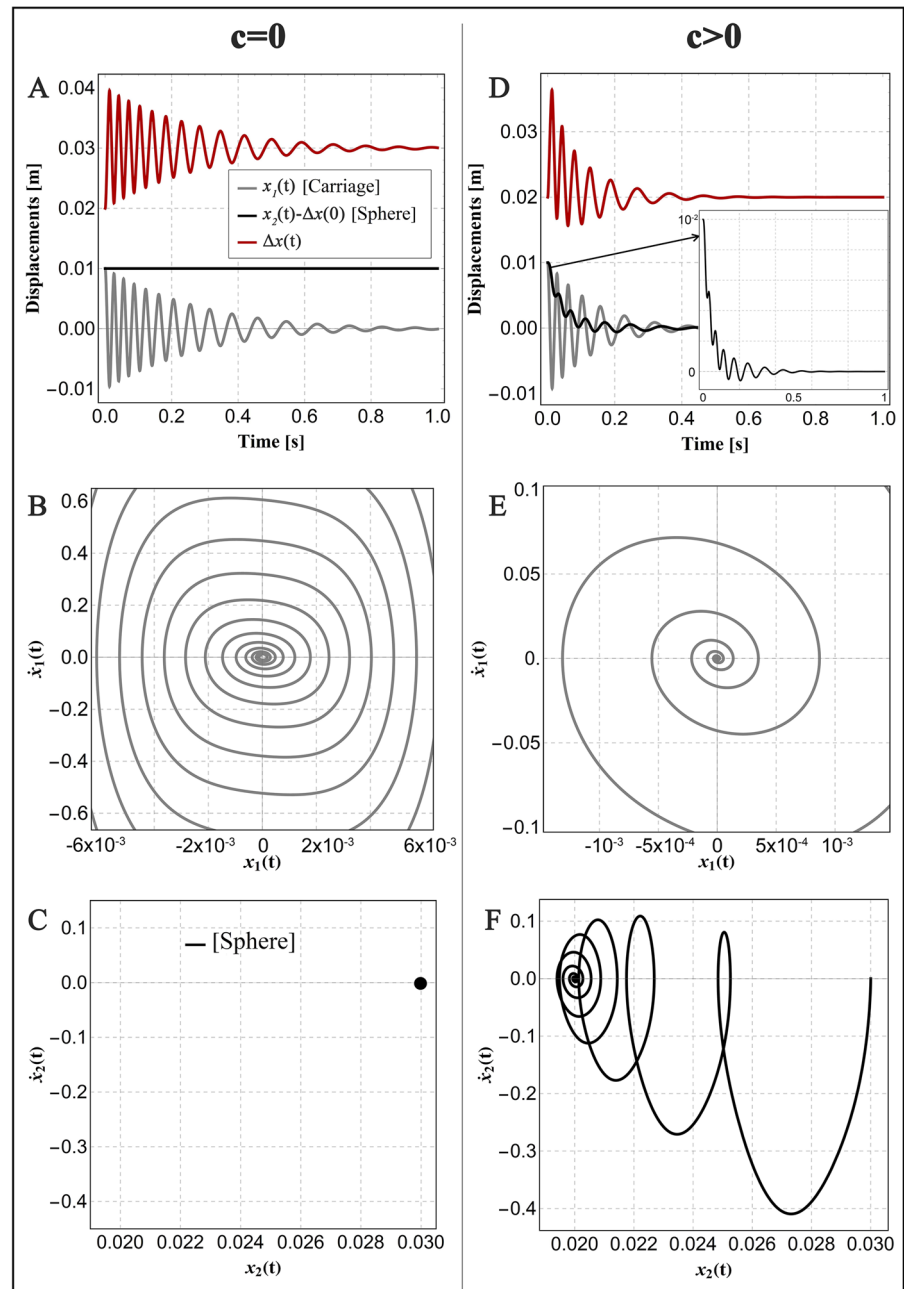
$$m_1 \ddot{x}_1(t) + d \dot{x}_1(t) + k_1 \left(\alpha + \beta x_1(t)^2 \right) x_1(t) - c (\dot{x}_2(t) - \dot{x}_1(t)) = 0, \tag{7}$$

$$m_2 \ddot{x}_2(t) + c (\dot{x}_2(t) - \dot{x}_1(t)) = 0, \tag{8}$$

α and β being the coefficients specifying the nonlinear behaviour of the springs. It is immediate to recognise that Eqs. (7)–(8) correspond to a damped Duffing oscillator [42–45] coupled to a linear oscillator.

By setting $\alpha = 1$, $\beta = 2 \times 10^6 \text{ m}^{-2}$, Fig. 6 shows the time histories and phase trajectories for both the two degrees of freedom. Notice that such a choice of parameters corresponds to the mono-stable Duffing model, which for $\beta = 0 \text{ m}^{-2}$ reproduces the linear behaviour already discussed in Sect. 2.1. On the contrary, the large value adopted for β in the numerical simulations pre-

Fig. 6 Displacements histories (A and D) and phase space plots for the carriage (B, E) and the sphere (C and F), by assuming $x_1(0) = 0.01$ m and $x_2(0) = x_1(0) + \Delta x(0) = 0.03$ m. In all graphics, the following parameters are assumed: $m_1 = 0.10$ kg, $m_2 = 0.04$ kg, $k_1 = 400$ N m⁻¹ and $d = 1$ N s m⁻¹. In graphics D, E and F, the damping parameter c is 1 N s m⁻¹



sented below is aimed at emphasising the effect of the cubic term. The other parameters are the same adopted in the linear case, and the initial conditions are those set in Eq. (6).

Interestingly, the nonlinear stiffness does not change the asymptotic behaviours of the system, by still distinguishing the two limit cases: indeed, for $c = 0$, Eqs. (7)–(8) are uncoupled and the sphere rests in its

initial position for any $t > 0$, while for $c > 0$ the sphere restores its initial relative position with respect to the centre of gravity of the carriage. In fact, by comparing plots Figs. 2A and E to 6A and D, respectively, it can be seen that, despite the oscillations of the two bodies in the nonlinear case are quite different with respect to the linear counterpart, the asymptotic behaviours registered are perfectly recovered.

3.2 Non-smooth friction

The assumption of damping linear with velocity used in Sects. 2.1 and 3.1 is physically plausible when a sphere moves on a smooth surface, and nonlinear phenomena are negligible. While, for the problem under investigation, the predictions of such a simple model have been confirmed by the experimental tests reported in Sect. 2.2, in order to analyse more general systems, a nonlinear dissipation model is here considered, while the linear elasticity of the springs is retained.

In order to define a mutual nonlinear damping term that upgrades the linear one utilised in Eqs. (1)–(2), i.e. $f_L^D(\dot{\xi}) = c \dot{\xi}$, being ξ a dummy variable (for instance, in Eqs. (1)–(2), $\xi = \dot{x}_2 - \dot{x}_1$), the dry friction model [46–48] has been selected. Within this framework, let us consider a body resting on a rough surface under the action of an increasing external force. Before the body starts sliding, friction and external force are in equilibrium, the latter do not exceeding the static friction. Whenever the latter is overcome by a large enough applied force, then the friction decreases to the kinetic value [55]. Hence, by introducing the dimensionless stick (static) and slip (kinetic) friction coefficients μ_1 and μ_2 , with $0 < \mu_2 \leq \mu_1$, the mutual nonlinear damping force in Eqs. (1)–(2) is replaced with

$$f_{NL}^D(\dot{\xi}) = \frac{\mu_1 F_N}{v_r} \dot{\xi} + (2(\mu_2 F_N - \chi v_r) \mathcal{H}(\dot{\xi}) - \frac{F_N}{v_r} (\mu_1 \dot{\xi} + \mu_2 v_r) + \chi (\dot{\xi} + v_r)) \mathcal{H}(|\dot{\xi}| - v_r). \tag{9}$$

Terms in Eq. (9) comment as follows: $\mathcal{H}(\cdot)$ is the Heaviside unit step function equal to 0 for negative values of its argument and 1 otherwise, F_N is the weight of the sphere (here acting normally to direction of the motion), $v_r > 0$, is the threshold reference velocity responsible for the transition from stick to slip behaviour of the dry friction [56–58], $\chi \geq 0$ is a damping parameter having dimensions of mass per time, as c in the linear case.

We emphasise that Eq. (9) approximates different friction models. In the limit $v_r \rightarrow 0^+$ and setting $\chi = 0$, Eq. (9) recovers the Amontons–Coulomb for $\mu_1 = \mu_2$, and the *stiction* friction model for $\mu_1 > \mu_2$ [59], both of which result in constant forces either for negative or positive velocities. However, for many different materials, friction has been experimentally shown to be velocity-strengthening [60], with a

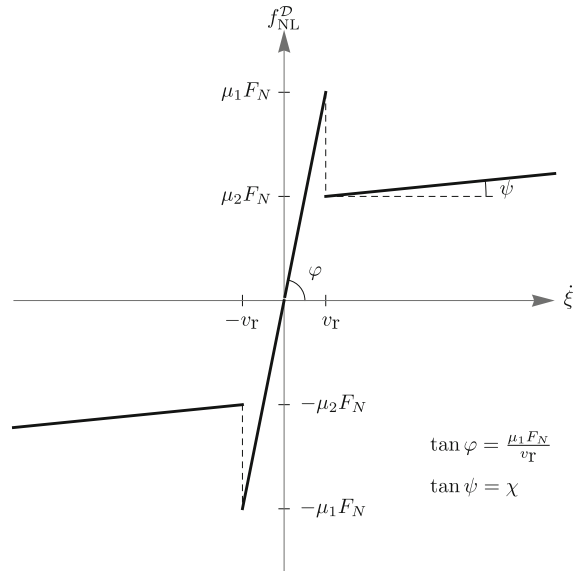


Fig. 7 Qualitative graph of f_{NL}^D for $\mu_1 > \mu_2$ and $\chi > 0$

viscous-like damping becoming dominant [61], indeed simulated by Eq. (9) by setting $\chi > 0$.

A qualitative graph of Eq. (9) is shown in Fig. 7.

The numerical integration of

$$m_1 \ddot{x}_1(t) + d \dot{x}_1(t) + k_1 x_1(t) + f_{NL}^D(\dot{x}_1(t) - \dot{x}_2(t)) = 0, \tag{10}$$

$$m_2 \ddot{x}_2(t) + f_{NL}^D(\dot{x}_2(t) - \dot{x}_1(t)) = 0, \tag{11}$$

in the time range $t_{\min} = 0$ s to $t_{\max} = 10^3$ s for a given set of mechanical parameters and the initial conditions reported in Eq. (6) allows plotting time histories, in terms of displacements and velocities, and phase trajectories elucidating that the stick–slip phenomenon arising between m_1 and m_2 strongly influences the oscillation of the overall system to a drastic change in its asymptotic behaviours.

In fact, unlike what happens in the previously analysed systems, the asymptotic binary behaviour is not confirmed in the general case. Let us consider the example shown in Fig. 8: despite x_1 asymptotically approaches 0 (Fig. 8A and C), the sphere does not invariably reach a rest position recovering the initial relative distance from the centre of gravity of the carriage (Fig. 8A and D), because of the strong nonlinear effect that arises in the first 0.2 s of the motion, during which the displacement and velocity histories of the sphere show stick phases alternating to slip motion

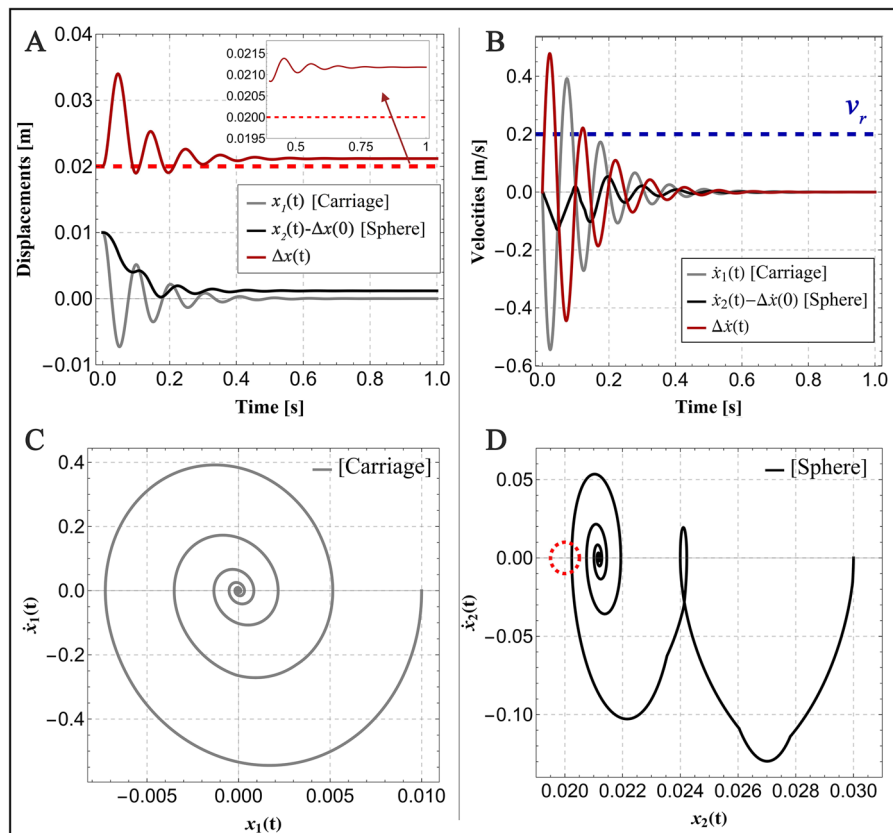


Fig. 8 Time histories, in terms of displacements (**A**) and velocities (**B**), and phase trajectories for the primary (**C**) and secondary mass (**D**). Initial conditions $x_1(0) = 0.01$ m and $x_2(0) = x_1(0) + \Delta x(0) = 0.03$ m are set. In all graphics, the following parameters are adopted: $m_1 = 0.10$ kg, $m_2 = 0.04$ kg, $k_1 = 400$ N m $^{-1}$ and $d = 1$ N s m $^{-1}$. The parameters of the nonlinear

dry friction model are set as follows: $\mu_1 = 0.509$, $\mu_2 = \mu_1/2$, $F_N = 0.3924$ N, $v_r = 0.2$ m s $^{-1}$. The red dashed line in plot (**A**) marks the asymptotic behaviour of the linear counterpart of the system, and the dashed circle in plot (**D**) highlights the point of coordinates (0.02, 0.00) corresponding to the attractor in the damped linear case

(Fig. 8A and B). Notice that the change in the velocity slope and the kinks in the phase trajectories are related to the change in the friction coefficient at $\dot{\xi} = v_r$.

However, it must be emphasised that if the relative velocity $\dot{\xi}$ does not overcome the value of v_r , the system essentially recovers the linear behaviour, as shown in Fig. 9. Reported results correspond to the numerical integration of Eqs. (10)–(10) by setting initial conditions tailored to ensure $\dot{\xi} < v_r$, having the same $\Delta x(0)$ and initial velocities, but $x_1(0)$ halved with respect to Eq. (6),

$$\begin{aligned} x_1(0) &= 5 \times 10^{-3} \text{ m,} \\ x_2(0) &= x_1(0) + \Delta x(0) = 0.025 \text{ m,} \\ \dot{x}_1(0) &= \dot{x}_2(0) = 0 \text{ m s}^{-1}. \end{aligned} \quad (12)$$

Furthermore, the same behaviour of the linear system can be obtained playing with the value of the parameter v_r , as shown Fig. 10 through two bifurcation diagrams. Such diagrams are built by integrating the equation of motion for the initial conditions given in Eq. (6) and a fixed set of parameters, at threshold velocity in the range 10^{-6} m s $^{-1} \leq v_r \leq 1$ m s $^{-1}$ (with a step of 10^{-3} m s $^{-1}$). It can be recognised that a critical value $v_{r,\text{crit}}$ can be detected ($v_{r,\text{crit}} \approx 0.4635$ m s $^{-1}$ for the parameters chosen in the numerical computations) below which (i.e. $v_r < v_{r,\text{crit}}$) the asymptotic value of Δx is different from $\Delta x(0)$, apart for a limited number of specific values of v_r , while, for any $v_r \geq v_{r,\text{crit}}$, $\Delta x(t)$ asymptotically approaches $\Delta x(0)$, as in the linear case (see Fig. 10). Such a behaviour is confirmed for different values of the dynamic viscosity χ (Fig. 10A)

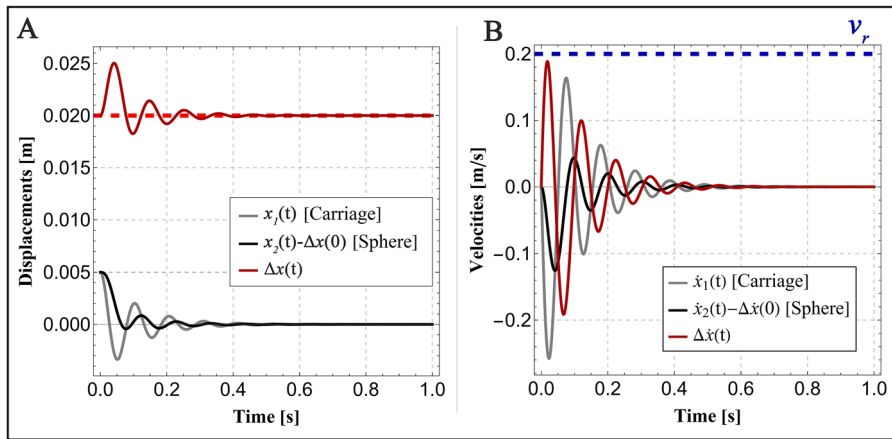
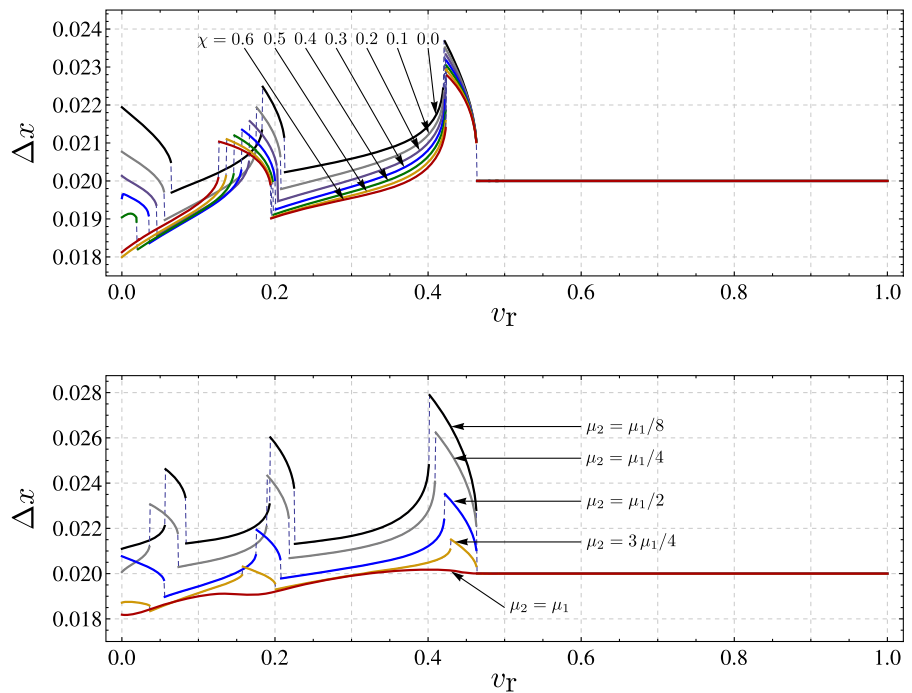


Fig. 9 Time histories, in terms of displacements (A) and velocities (B). Initial conditions $x_1(0) = 0.005$ m and $x_2(0) = x_1(0) + \Delta x(0) = 0.025$ m are set. In all graphics, the following parameters are adopted: $m_1 = 0.10$ kg, $m_2 = 0.04$ kg, $k_1 = 400$ N m⁻¹ and $d = 1.00$ N s m⁻¹. The parameters of the non-

linear dry friction model are set as follows: $\mu_1 = 0.5097$, $\mu_2 = \mu_1/2$, $F_N = 0.3924$ N, $v_r = 0.2$ m s⁻¹. Notice that, to compare results with those obtained in the linear case, the parameters are set to fulfil $\mu_1 F_N/v_r = c$

Fig. 10 Bifurcation diagrams showing as the asymptotic value of Δx varies in function of v_r , for the parameters set as:
 $m_1 = 0.10$ kg,
 $m_2 = 0.04$ kg,
 $k_1 = 400$ N m⁻¹,
 $d = 1.00$ N s m⁻¹,
 $F_N = 0.3924$ N,
 $\mu_1 = 0.51$, $x_1(0) = 0.01$ m,
 $x_2(0) = x_1(0) + \Delta x(0)$,
 $\Delta x(0) = 0.02$ m,
 $\dot{x}_1(0) = \dot{x}_2(0) = 0$ m s⁻¹.
 The top panel A reports diagrams built by setting the dynamic friction coefficient $\mu_2 = \mu_1/2$ and for seven different values of the dynamic viscosity χ . The bottom panel B shows diagrams for the damping coefficient $\chi = 0.10$ N s m⁻¹ and five different values of the ratio μ_2/μ_1



and the friction ratio μ_2/μ_1 (Fig. 10B). The latter diagram also elucidates that whenever $\mu_2 < \mu_1$ the bifurcation diagram contains jumps, for certain values of $v_r < v_{r,crit}$, becoming smaller and smaller as μ_2 approaches μ_1 .

4 Tunable elastic constraints on moving mass: back to standard behaviours

As a final example, let us consider the system shown in Fig. 11, which is the same as that shown in Fig. 1, except that here the sphere is anchored to the carriage by means

of two elastic springs of stiffness k_{2L} and k_{2R} , which are assumed to be tunable through pre-stretching.

The equations of motion are written as

$$m_1 \ddot{x}_1(t) + d \dot{x}_1(t) + k_1 x_1(t) - c (\dot{x}_2(t) - \dot{x}_1(t)) - (k_{2L} + k_{2R}) (x_2(t) - x_1(t)) = 0, \tag{13}$$

$$m_2 \ddot{x}_2(t) + c (\dot{x}_2(t) - \dot{x}_1(t)) + (k_{2L} + k_{2R}) \times (x_2(t) - x_1(t)) = 0. \tag{14}$$

In order k_{2L} and k_{2R} are tunable, we consider an incompressible Neo–Hookean constitutive law [62, 63], which allows writing

$$k_{2L} = k_0 \left(1 + 2\lambda_{2L}^{-3}\right), \tag{15}$$

$$k_{2R} = k_0 \left(1 + 2\lambda_{2R}^{-3}\right),$$

where k_0 represents a constant parameter related to the geometrical and mechanical characteristics of the springs and $\lambda_{2L} = l_{2L}/l_0$ and $\lambda_{2R} = l_{2R}/l_0$ indicate, respectively, the longitudinal stretches of springs set on the left and right side of the sphere, being l_0 the rest length and l_{2L} and l_{2R} the current lengths. Notice that, in the small-on-large hypothesis, the current length remains substantially equal to the mounting length, that is the distance between the sphere and the clamp (see Fig. 11). In addition to pre-stretch the spring, we assume $l_{2L} > l_0$ and $l_{2R} > l_0$. Here, since the rest length of both springs is the same, for the self-equilibrium condition, the stretches λ_{2L} and λ_{2R}

are coincident ($\lambda_{2L} = \lambda_{2R} = \lambda_2$) and the sphere is placed exactly in the middle of the carriage (Fig. 11), i.e. $\Delta x(0) = 0$ m. Conversely, springs having different rest lengths imply not null relative position of the sphere with respect to the centre of gravity of the carriage.

By setting $y_1(t) = \dot{x}_1(t)$ and $y_2(t) = \dot{x}_2(t)$, Eqs. (13)–(14) can be conveniently rearranged in matrix form as

$$\begin{pmatrix} \dot{x}_1 \\ \dot{x}_2 \\ \dot{y}_1 \\ \dot{y}_2 \end{pmatrix} = \begin{pmatrix} 0 & 0 & 1 & 0 \\ 0 & 0 & 0 & 1 \\ -(k_1 + k_2)m_1^{-1} & k_2 m_1^{-1} & -(c + d)m_1^{-1} & c m_1^{-1} \\ k_2 m_2^{-1} & -k_2 m_2^{-1} & c m_2^{-1} & -c m_2^{-1} \end{pmatrix} \begin{pmatrix} x_1 \\ x_2 \\ y_1 \\ y_2 \end{pmatrix}, \tag{16}$$

where, for the sake of simplicity, $k_2 = k_{2L} + k_{2R}$ is set and the time dependence is implied. The characteristic equation associated to Eq. (3) is written as

$$m_1 m_2 \gamma^4 + (c(m_1 + m_2) + d m_2) \gamma^3 + (cd + k_1 m_2 + (m_1 + m_2) k_2) \gamma^2 + (ck_1 + dk_2) \gamma + k_1 k_2 = 0, \tag{17}$$

solvable in closed form [49]. For the range of parameters of interest, the algebraic multiplicity of each eigenvalue is 1. Therefore, a complete system of 4 eigenvectors can be provided. The general integral of Eq. (16), i.e. $\mathbf{z}(t) \equiv (x_1(t), x_2(t), y_1(t), y_2(t))^T$, can be obtained as

Fig. 11 2-DOF model of a spherical mass attached to a sliding carriage through pre-stretched nonlinear springs

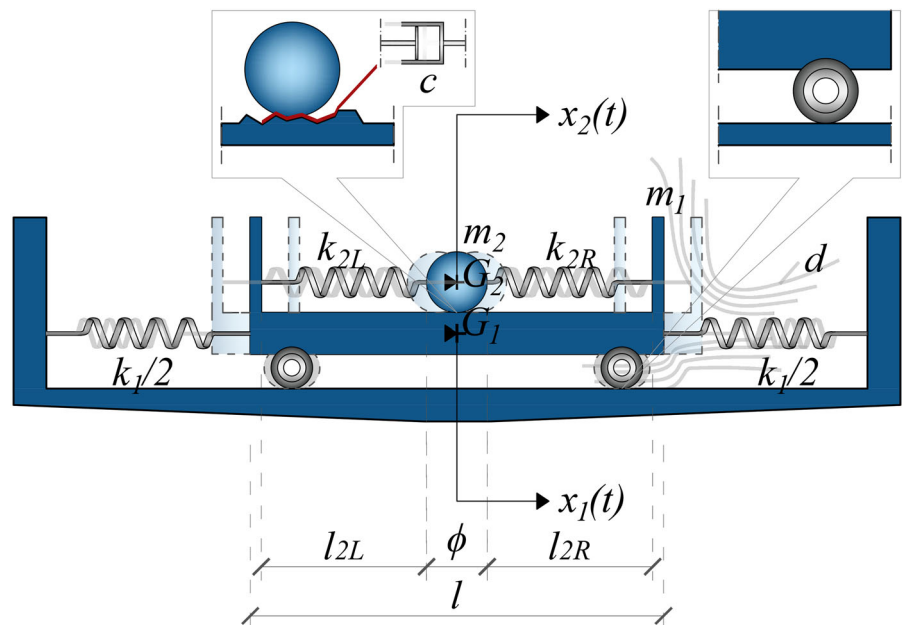
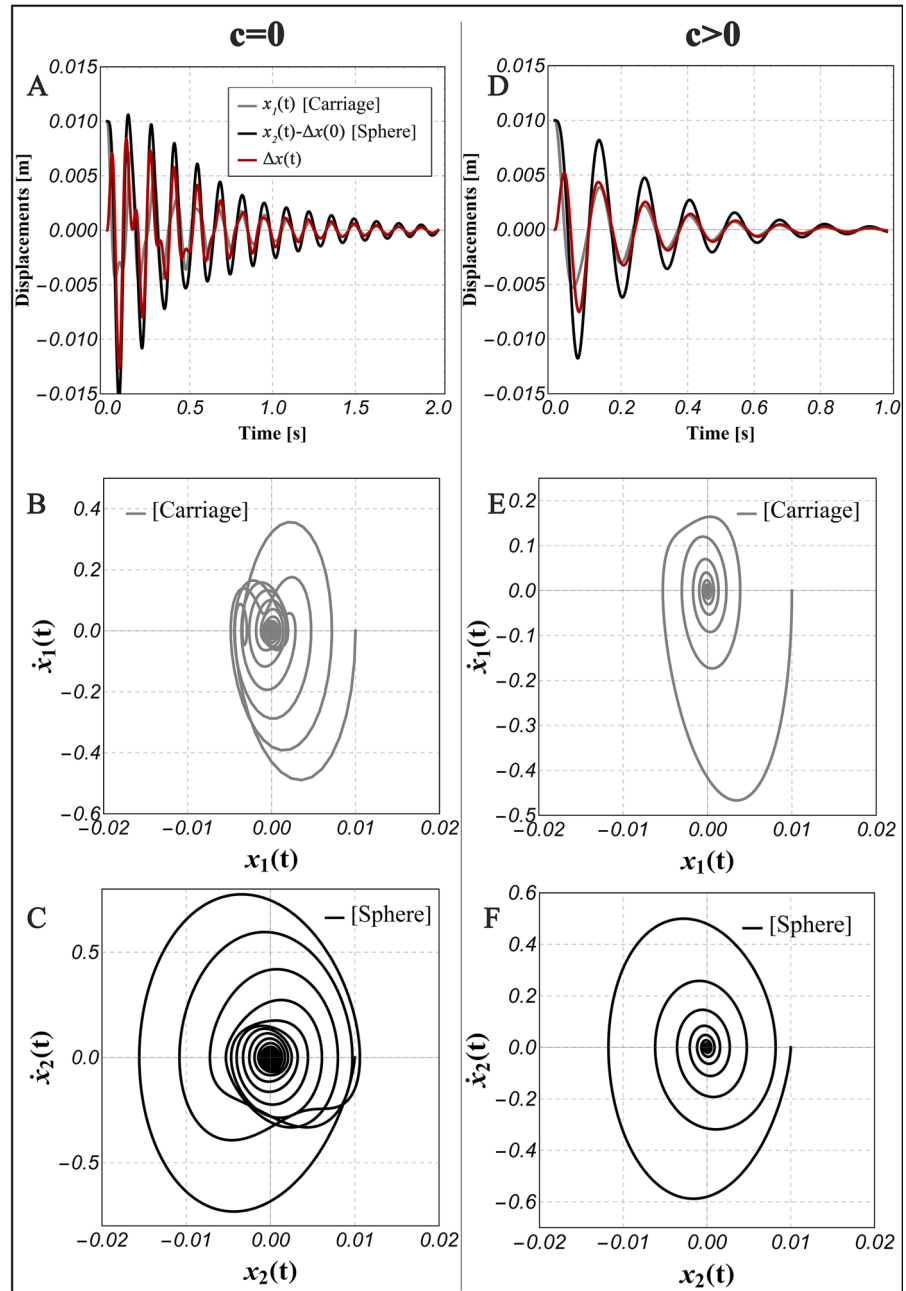


Fig. 12 Displacement histories (A and D) and phase space plots (B, C, E and F) of the 2-DOF system made up of a spherical mass attached to the carriage through pre-stretched springs. In all graphics, the following parameters are assumed: $m_1 = 0.10$ kg, $m_2 = 0.04$ kg, $k_0 = 50$ N m⁻¹, $k_1 = 400$ N m⁻¹, $\lambda_2 = 1.5$, $d = 1$ N s m⁻¹. In the graphics D, E and F the damping parameter $c = 1$ N s m⁻¹ is set



$$\mathbf{z}(t) = d_1 \mathbf{w}_1 e^{\gamma_1 t} + d_2 \mathbf{w}_2 e^{\gamma_2 t} + d_3 \mathbf{w}_3 e^{\gamma_3 t} + d_4 \mathbf{w}_4 e^{\gamma_4 t}, \tag{18}$$

being \mathbf{w}_i , $i = \{1, \dots, 4\}$, the eigenvectors associated to eigenvalues γ_i , and d_i represent the constants of integration depending on initial conditions. For the sake of brevity, the explicit expressions of eigenvalues and eigenvectors of Eq. (16) are given in Appendix A.

Based on the analytical solution given by Eq. (18), the displacement histories and the phase trajectories are provided in Fig. 12, for the initial conditions set as

$$\begin{aligned} x_1(0) &= x_2(0) = 0.01 \text{ m,} \\ \dot{x}_1(0) &= \dot{x}_2(0) = 0 \text{ m s}^{-1}. \end{aligned} \tag{19}$$

By examining all graphics reported in Fig. 12, one can observe that the binary asymptotic behaviour of the previous case is not confirmed.

In particular, for the system under investigation, a single asymptotic behaviour occurs: both the carriage and the sphere return to their initial position, related to the presence of the nonlinear pre-stretched springs, which maintain coupled the dynamics of the sphere and the carriage, also in the limit case of vanishing damping. However, despite the unique asymptotic behaviour in this last case may be somewhat expected, the possibility of modulating the pre-stress in the springs attached to the sphere can be interestingly exploited in order to emphasise some dynamic effects on the overall system; for instance, by properly tuning the nonlinear stiffness of the sphere, a reduction of the dynamic amplification of the carriage can be obtained, thus inducing a mass-damping effect on it.

5 Conclusions and perspectives

Although the problems of moving masses or loads have been addressed in the inherent literature over the years, somehow surprisingly no research paper focuses on the asymptotic behaviour of the simplest “toy system” case of an elastically constrained rigid system surmounted by a movable mass.

To face this issue, in the present paper, analytical solutions and numerical results were provided, by making reference to a 2-DOF model. The results were compared to experimental findings obtained by *ad hoc* designed and built-up prototype undergoing conditions that reproduced the mechanical response of the idealised structure. All the outcomes confirmed the non-trivial asymptotic behaviour predicted by theory and observed in the laboratory for different masses. In particular, when nonzero friction at the sphere–carriage interface is considered and other nonlinear phenomena can be neglected, the spherical mass counterintuitively returns to the arbitrarily prescribed relative sphere–carriage initial position. On the contrary, if the friction at the sphere–carriage interface vanishes, a second complementary behaviour occurs, that is the sphere holds its initial position over the entire observation time, regardless the vibration history of the support, this duality here called *binary*.

Furthermore, it was numerically shown that nonlinear elastic springs constraining the carriage do not change this binary asymptotic behaviour, while it can be either maintained or lost, depending on parameters or initial conditions if nonlinear friction phenomena are

incorporated into the model for taking into account, for instance, stick–slip processes occurring at the interface. Also, it was found that additional elastic constraints applied to the spherical mass back the system to a standard behaviour. Apart from the value of the work *per se*, it is felt that the results could be helpfully employed for different engineering applications in order to design new optimal tuned mass dampers, also by exploiting the effects of nonlinearities.

Author contributions MA contributed to methodology, software, validation, formal analysis, investigation, data curation, writing, review and editing, and visualisation. AC contributed to methodology, experimental validation, investigation, data curation, and visualisation. EB contributed to methodology, software, validation, formal analysis, investigation, writing, review and editing, and visualisation. ARC contributed to methodology and formal analysis and supported validation and investigation. MF contributed with conceptualisation, methodology, investigation, review and editing, supervised the project and provided funding acquisition.

Funding Open access funding provided by Università degli Studi di Napoli Federico II within the CRUI-CARE Agreement. MF acknowledges the support of the Italian Ministry of University and Research (MUR) through the grants STREAM ARS01_01182, the PRIN-20177TTP3S and the grant FIT4MEDROB (PNC0000007). MA acknowledges the support of the Italian Ministry of University and Research (MUR) through the PNRR grant SAMOTHRACE (B73C22000810001, Spoke 3, coordinated by prof. M. Zingales).

Data availability No data were used for the research described in the article.

Declarations

Conflict of interest The authors declare that they have no known competing financial interests or personal relationships that could have appeared to influence the work reported in this paper.

Open Access This article is licensed under a Creative Commons Attribution 4.0 International License, which permits use, sharing, adaptation, distribution and reproduction in any medium or format, as long as you give appropriate credit to the original author(s) and the source, provide a link to the Creative Commons licence, and indicate if changes were made. The images or other third party material in this article are included in the article’s Creative Commons licence, unless indicated otherwise in a credit line to the material. If material is not included in the article’s Creative Commons licence and your intended use is not permitted by statutory regulation or exceeds the permitted use, you will need to obtain permission directly from the copyright holder. To view a copy of this licence, visit <http://creativecommons.org/licenses/by/4.0/>.

Appendix

Here, for the sake of completeness, we report the eigenvalues and eigenvectors of Eqs. (3) and (16).

The eigenvalues of Eq. (3) are

$$\begin{aligned} \eta_1 &= 0, \\ \eta_2 &= \frac{(\sqrt{G} + H)^{1/3}}{3 \cdot 2^{1/3}} - \frac{2^{1/3}L}{(\sqrt{G} + H)^{1/3}} - I, \\ \eta_{3,4} &= \frac{(1 \pm j\sqrt{3})L}{2^{2/3}(\sqrt{G} + H)^{1/3}} - \frac{(1 \mp j\sqrt{3})(\sqrt{G} + H)^{1/3}}{6 \cdot 2^{1/3}} - I, \end{aligned} \tag{20}$$

$$M = \sqrt{(1 + \eta_i^2) \left(k_1^2 + 2k_1\eta_i(c + d + m_1\eta_i) + \eta_i^2(2c^2 + 2c(d + m_1\eta_i) + (d + m_1\eta_i)^2) \right)}. \tag{23}$$

where j is the imaginary unit and G, H, I and L are evaluated, respectively, as

$$\begin{aligned} G &= \frac{27}{m_1^4 m_2^4} \left(4c^4 k_1 m_1^3 + m_2^2 (c + d)^2 \right. \\ &\quad \times \left(k_1 m_2 (2c(2c + d) - k_1 m_2) - c^2 d^2 \right) \\ &\quad + c^2 m_1^2 \left(4k_1 m_2 (c(3c - 2d) \right. \\ &\quad \left. + 2k_1 m_2) - c^2 d^2 \right) + 2m_1 m_2 \\ &\quad \times \left(k_1 m_2 (c^2 (6c^2 + cd + d^2) + 2k_1 m_2 \right. \\ &\quad \left. \times (k_1 m_2 - c(5c + 2d))) - c^3 d^2 (c - d) \right) \Big), \\ H &= -\frac{2(c + d)^3}{m_1^3} - \frac{3(c + d)(c(2c - d) - 3k_1 m_2)}{m_1^2 m_2} \\ &\quad - \frac{3c(c(2c - d) + 6k_1 m_2)}{m_1 m_2^2} - \frac{2c^3}{m_2^3}, \\ I &= \frac{c(m_1 + m_2) + dm_2}{3m_1 m_2}, \\ L &= \frac{3m_1 m_2 (cd + k_1 m_2) - (c(m_1 + m_2) + dm_2)^2}{3m_1^2 m_2^2}. \end{aligned} \tag{21}$$

The components of the i th eigenvector $\mathbf{v}_i \equiv (v_{1i}, v_{2i}, v_{3i}, v_{4i})^T$ of Eqs. (1) and (2), being the subscript $i = \{1, \dots, 4\}$ referred to i th eigenvalue, are

$$\begin{aligned} v_{1i} &= \frac{c\eta_i}{M}, \\ v_{2i} &= \frac{k_1 + \eta_i(c + d + m_1\eta_i)}{M}, \\ v_{3i} &= \frac{c\eta_i^2}{M}, \\ v_{4i} &= \frac{\eta_i(k_1 + \eta_i(c + d + m_1\eta_i))}{M}, \end{aligned} \tag{22}$$

where M can be made explicit as

By substituting, in Eqs. (22) and (23), η_i with the i th ($i = 1, \dots, 4$) eigenvalue given by Eq. (20), taking into account Eq. (21), the closed-form expressions of the eigenvectors components given by can be made explicit.

The eigenvalues of the system (16) are

$$\begin{aligned} \gamma_{1,2} &= -\frac{g_3}{4g_4} - \frac{1}{2} \sqrt{\frac{g_3^2}{4g_4^2} + \frac{N^{1/3}}{32^{1/3}g_4} - \frac{2g_2}{3g_4} + \frac{P}{g_4}} \\ &\quad \mp \frac{1}{2} \sqrt{\frac{g_3^2}{2g_4^2} - \frac{N^{1/3}}{32^{1/3}g_4} - \frac{4g_2}{3g_4} - \frac{P}{g_4} - Q}, \\ \gamma_{3,4} &= \mp \frac{g_3}{4g_4} + \frac{1}{2} \sqrt{\frac{g_3^2}{4g_4^2} + \frac{N^{1/3}}{32^{1/3}g_4} - \frac{2g_2}{3g_4} + \frac{P}{g_4}} \\ &\quad \mp \frac{1}{2} \sqrt{\frac{g_3^2}{2g_4^2} - \frac{N^{1/3}}{32^{1/3}g_4} - \frac{4g_2}{3g_4} - \frac{P}{g_4} + Q}, \end{aligned} \tag{24}$$

being the coefficients N, P and Q given by

$$\begin{aligned}
N &= 2g_2^3 - 9g_1g_2g_3 + 27g_0g_3^2 + 27g_1^2g_4 - 72g_0g_2g_4 \\
&\quad + \sqrt{(2g_2^3 - 9g_1g_2g_3 + 27g_0g_3^2 + 27g_1^2g_4 - 72g_0g_2g_4)^2 - 4(g_2^2 - 3g_1g_3 + 12g_0g_4)^3}, \\
P &= \frac{2^{1/3}(g_2^2 - 3g_1g_3 + 12g_0g_4)}{3N^{1/3}}, \quad Q = \frac{4g_2g_3g_4 - 8g_1g_4^2 - g_3^3}{4g_4^2\sqrt{3}2^{2/3}g_3^2 + 6g_4N^{1/3} - 2^{11/3}g_2g_4 + 32^{8/3}g_4P}, \quad (25)
\end{aligned}$$

and the parameters g_i

$$\begin{aligned}
g_0 &= k_1k_2, \\
g_1 &= ck_1 + dk_2, \\
g_2 &= cd + k_1m_2 + k_2(m_1 + m_2), \\
g_3 &= cm_1 + m_2(c + d), \\
g_4 &= m_1m_2. \quad (26)
\end{aligned}$$

The components of the i th eigenvector $\mathbf{w}_i \equiv (w_{1i}, w_{2i}, w_{3i}, w_{4i})^T$ of Eqs. (13) and (14), with the subscript $i = \{1, \dots, 4\}$ referred to i th eigenvalue, can be provided as

$$\begin{aligned}
w_{1i} &= \frac{c\gamma_i + m_2\gamma_i^2 + k_2}{R}, \\
w_{2i} &= \frac{c\gamma_i + k_2}{R}, \\
w_{3i} &= \frac{\gamma_i(c\gamma_i + m_2\gamma_i^2 + k_2)}{R}, \\
w_{4i} &= \frac{\gamma_i(c\gamma_i + k_2)}{R}, \quad (27)
\end{aligned}$$

with

$$R = \frac{1}{\sqrt{(1 + \gamma_i^2)(2cm_2\gamma_i^3 + m_2^2\gamma_i^4 + 4c\gamma_ik_2 + 2k_2^2 + 2\gamma_i^2(c^2 + m_2k_2))}}. \quad (28)$$

By replacing, in Eqs. (27) and (28), γ_i with the i th ($i = 1, \dots, 4$) eigenvalue given by Eq. (24), taking into account Eqs. (25) and (26), the components of the eigenvectors can be written in explicit form.

References

1. Timoshenko, S.P.: On the forced vibrations of bridges. Lond. Edinb. Dublin Philos. Mag. J. Sci. **43**(257), 1018–1019 (1922). <https://doi.org/10.1080/14786442208633953>
2. Smith, C.E.: Motions of a stretched string carrying a moving mass particle. J. Appl. Mech. **31**(1), 29–37 (1964). <https://doi.org/10.1115/1.3629566>
3. Steele, C.: The finite beam with a moving load. J. Appl. Mech. **34**(1), 111–118 (1967). <https://doi.org/10.1115/1.3607609>
4. Nelson, H.D., Conover, R.: Dynamic stability of a beam carrying moving masses. J. Appl. Mech. **38**(4), 1003–1006 (1971). <https://doi.org/10.1115/1.3408901>
5. Stanišić, M., Euler, J., Montgomery, S.: On a theory concerning the dynamical behavior of structures carrying moving masses. Ingenieur Arch. **43**(5) (1974)
6. Blejwas, T., Feng, C., Ayre, R.: Dynamic interaction of moving vehicles and structures. J. Sound Vib. **67**(4), 513–521 (1979)
7. Stanišić, M.: On a new theory of the dynamic behavior of the structures carrying moving masses. Ingenieur Arch. **55**(3), 176–185 (1985)
8. Sadiku, S., Leipholz, H.: On the dynamics of elastic systems with moving concentrated masses. Ingenieur Arch. **57**(3), 223–242 (1987)
9. Olsson, M.: On the fundamental moving load problem. J. Sound Vib. **145**(2), 299–307 (1991)
10. Fraldi, M., Cutolo, A., Carotenuto, A.R., Palumbo, S., Pugno, N.: A lesson from earthquake engineering for selectively damaging cancer cell structures. J. Mech. Behav. Biomed. Mater. **119**, 104533 (2021)
11. Fryba, L.: Vibration of Solids and Structures Under Moving Loads vol. 1. Springer, Dordrecht (2013). <https://doi.org/10.1007/978-94-011-9685-7>
12. Dehestani, M., Mofid, M., Vafai, A.: Investigation of critical influential speed for moving mass problems on beams. Appl. Math. Model. **33**(10), 3885–3895 (2009)
13. Ting, E., Genin, J., Ginsberg, J.: A general algorithm for moving mass problems. J. Sound Vib. **33**(1), 49–58 (1974)
14. Lee, H.: On the dynamic behaviour of a beam with an accelerating mass. Arch. Appl. Mech. **65**(8), 564–571 (1995)
15. Michaltsos, G., Sophianopoulos, D., Kounadis, A.: The effect of a moving mass and other parameters on the dynamic response of a simply supported beam. J. Sound Vib. **191**(3), 357–362 (1996)
16. Lee, U.: Separation between the flexible structure and the moving mass sliding on it. J. Sound Vib. **209**(5), 867–877 (1998)

17. Gómez, B., Repetto, C., Stia, C., Welti, R.: Oscillations of a string with concentrated masses. *Eur. J. Phys.* **28**(5), 961 (2007)
18. Dyniewicz, B., Bajer, C.I.: General approach to problems with moving mass. *Transactions* **16**, 99–106 (2008)
19. Fonseca, C.A., de Paula, G., Pereira, M., Cunha Jr, A.: Analysis of vibrations on an aerial cable car system with moving mass. In: XVIII International Symposium on Dynamic Problems of Mechanics (Diname 2019) (2019)
20. Lee, Y.-H., Kim, S.-S.: Combined analytical and numerical solution for an elastically supported Timoshenko beam to a moving load. *J. Mech. Sci. Technol.* **28**(7), 2549–2559 (2014)
21. Aristoff, J.M., Clanet, C., Bush, J.W.: The elastochrone: the descent time of a sphere on a flexible beam. *Proc R. Soc. A: Math. Phys. Eng. Sci.* **465**(2107), 2293–2311 (2009)
22. Zhao, X., Van Der Heijden, G., Hu, Z.: Vibrations of beams and rods carrying a moving mass. In: *Journal of Physics: Conference Series*, vol. 721, p. 012016 (2016). IOP Publishing
23. Ferretti, M., Piccardo, G.: Dynamic modeling of taut strings carrying a traveling mass. *Continuum Mech. Thermodyn.* **25**(2), 469–488 (2013). <https://doi.org/10.1007/s00161-012-0278-1>
24. Luongo, A., Piccardo, G.: Dynamics of taut strings traveled by train of forces. *Continuum Mech. Thermodyn.* **28**(1), 603–616 (2016). <https://doi.org/10.1007/s00161-015-0473-y>
25. Dyniewicz, B., Bajer, C.I.: Paradox of a particle's trajectory moving on a string. *Arch. Appl. Mech.* **79**(3), 213–223 (2009). <https://doi.org/10.1007/s00419-008-0222-9>
26. Gavrilov, S.N., Eremeyev, V.A., Piccardo, G., Luongo, A.: A revisit of the paradox of discontinuous trajectory for a mass particle moving on a taut string. *Nonlinear Dyn.* **86**(4), 2245–2260 (2016). <https://doi.org/10.1007/s11071-016-3080-y>
27. Ferretti, M., Gavrilov, S.N., Eremeyev, V.A., Luongo, A.: Nonlinear planar modeling of massive taut strings travelled by a force-driven point-mass. *Nonlinear Dyn.* **97**(4), 2201–2218 (2019). <https://doi.org/10.1007/s11071-019-05117-z>
28. Ferretti, M., Piccardo, G., dell'Isola, F., Luongo, A.: Dynamics of taut strings undergoing large changes of tension caused by a force-driven traveling mass. *J. Sound Vib.* **458**, 320–333 (2019). <https://doi.org/10.1016/j.jsv.2019.06.035>
29. Sung, Y.-G.: Modelling and control with piezoactuators for a simply supported beam under a moving mass. *J. Sound Vib.* **250**(4), 617–626 (2002)
30. Nikkhoo, A.: Investigating the behavior of smart thin beams with piezoelectric actuators under dynamic loads. *Mech. Syst. Signal Process.* **45**(2), 513–530 (2014)
31. Stancioiu, D., Ouyang, H.: Optimal vibration control of beams subjected to a mass moving at constant speed. *J. Vib. Control* **22**(14), 3202–3217 (2016)
32. Pi, Y., Ouyang, H.: Vibration control of beams subjected to a moving mass using a successively combined control method. *Appl. Math. Model.* **40**(5–6), 4002–4015 (2016)
33. Liu, X., Wang, Y., Ren, X.: Optimal vibration control of moving-mass beam systems with uncertainty. *J. Low Freq. Noise Vib. Act. Control* **39**(3), 803–817 (2020)
34. Wakaba, L., Balachandar, S.: On the added mass force at finite Reynolds and acceleration numbers. *Theoret. Comput. Fluid Dyn.* **21**(2), 147–153 (2007)
35. Wu, J.-Z., Lu, X.-Y., Zhuang, L.-X.: Integral force acting on a body due to local flow structures. *J. Fluid Mech.* **576**, 265–286 (2007)
36. Konstantinidis, E.: Added mass of a circular cylinder oscillating in a free stream. *Proc. R. Soc. A: Math. Phys. Eng. Sci.* **469**(2156), 20130135 (2013)
37. Yang, D.-H., Shin, J.-H., Lee, H., Kim, S.-K., Kwak, M.K.: Active vibration control of structure by active mass damper and multi-modal negative acceleration feedback control algorithm. *J. Sound Vib.* **392**, 18–30 (2017). <https://doi.org/10.1016/j.jsv.2016.12.036>
38. Love, J., Haskett, T.: The practical effects of friction for tuned mass dampers installed in tall buildings. *Eng. Struct.* **265**, 114495 (2022)
39. Bolotnik, N.N., Figurina, T.Y., Chernous'ko, F.L.: Optimal control of the rectilinear motion of a two-body system in a resistive medium. *J. Appl. Math. Mech.* **76**(1), 1–14 (2012). <https://doi.org/10.1016/j.jappmathmech.2012.03.001>
40. Nunuparov, A., Becker, F., Bolotnik, N., Zeidis, I., Zimmermann, K.: Dynamics and motion control of a capsule robot with an opposing spring. *Arch. Appl. Mech.* **89**(10), 2193–2208 (2019). <https://doi.org/10.1007/s00419-019-01571-8>
41. Nguyen, V.-D., La, N.-T.: An improvement of vibration-driven locomotion module for capsule robots. *Mech. Based Des. Struct. Mach.* **50**(5), 1658–1672 (2022). <https://doi.org/10.1080/15397734.2020.1760880>
42. Holmes, P., Rand, D.: Phase portraits and bifurcations of the non-linear oscillator: $\ddot{x} + (\alpha + \gamma x^2 + \beta x + \delta x^3) = 0$. *Int. J. Non-Linear Mech.* **15**(6), 449–458 (1980)
43. Nayfeh, A.H., Mook, D.T.: *Nonlinear Oscillations*. Wiley, Hoboken (2008)
44. Kovacic, I., Brennan, M.J.: *The Duffing Equation: Nonlinear Oscillators and Their Behaviour*. Wiley, Hoboken (2011)
45. Guckenheimer, J., Holmes, P.: *Nonlinear Oscillations, Dynamical Systems, and Bifurcations of Vector Fields*, vol. 42. Springer, New York (2013)
46. Elmer, F.-J.: Nonlinear dynamics of dry friction. *J. Phys. A: Math. Gen.* **30**(17), 6057 (1997)
47. Sextro, W., Poli, C.: Dynamical contact problems with friction: Models, methods, experiments and applications. *Lecture notes in applied mechanics* vol. 3. *Appl. Mech. Rev.* **56**(1), 2–3 (2003)
48. Chen, G.S.: *Handbook of Friction-Vibration Interactions*. Woodhead Publishing, Cambridge (2014)
49. Chávez-Pichardo, M., Martínez-Cruz, M.A., Trejo-Martínez, A., Vega-Cruz, A.B., Arenas-Resendiz, T.: On the practicality of the analytical solutions for all third- and fourth-degree algebraic equations with real coefficients. *Mathematics* **11**(6), 1447 (2023). <https://doi.org/10.3390/math11061447>
50. Argenziano, M., Faiella, D., Carotenuto, A., Mele, E., Fraldi, M.: Generalization of the Den Hartog model and rule-of-thumb formulas for optimal tuned mass dampers. *J. Sound Vib.* **538**, 117213 (2022)
51. Markus, L.: Structurally stable differential systems. *Ann. Math.* **73**(1), 1–19 (1961)
52. Siemens: SolidEdge v. 2019. <https://solidedge.siemens.com/>

53. Wolfram Research, Inc.: Mathematica, Version 13.2. Champaign, IL, 2022. <https://www.wolfram.com/mathematica>
54. Sofroniou, M., Knapp, R.: Advanced Numerical Differential Equation Solving in Mathematica. Wolfram Mathematica tutorial collection, Wolfram Research Inc. (2008). Currently available at: <https://library.wolfram.com/infocenter/Books/8503/>. Accessed on 15 January 2023
55. Kligerman, Y., Varenberg, M.: Elimination of stick-slip motion in sliding of split or rough surface. *Tribol. Lett.* **53**(2), 395–399 (2014). <https://doi.org/10.1007/s11249-013-0278-8>
56. Heslot, F., Baumberger, T., Perrin, B., Caroli, B., Caroli, C.: Creep, stick-slip, and dry-friction dynamics: experiments and a heuristic model. *Phys. Rev. E* **49**(6), 4973 (1994)
57. Awrejcewicz, J., Olejnik, P.: Occurrence of stick-slip phenomenon. *J. Theor. Appl. Mech.* **45**(1), 33–40 (2007)
58. Pust, L., Pešek, L., Radolfová, A.: Various types of dry friction characteristics for vibration damping. *Eng. Mech.* **18**(3–4), 203–224 (2011)
59. Leine, R.I., Nijmeijer, H.: *Modelling of Dry Friction*, pp. 39–46. Springer, Berlin (2004). https://doi.org/10.1007/978-3-540-44398-8_4
60. Bar-Sinai, Y., Spatschek, R., Brener, E.A., Bouchbinder, E.: Velocity-strengthening friction significantly affects interfacial dynamics, strength and dissipation. *Sci. Rep.* **5**(1), 7841 (2015). <https://doi.org/10.1038/srep07841>
61. Morrow, R., Grant, A., Jackson, D.P.: A strange behavior of friction. *Phys. Teacher* **37**(7), 412–415 (1999). <https://doi.org/10.1119/1.880335>
62. Palumbo, S., Carotenuto, A.R., Cutolo, A., Deseri, L., Fraldi, M.: Nonlinear elasticity and buckling in the simplest soft-strut tensegrity paradigm. *Int. J. Non-Linear Mech.* **106**, 80–88 (2018)
63. Palumbo, S., Carotenuto, A., Cutolo, A., Owen, D., Deseri, L., Fraldi, M.: Bulky auxeticity, tensile buckling and deck-of-cards kinematics emerging from structured continua. *Proc. R. Soc. A* **477**(2246), 20200729 (2021)

Publisher's Note Springer Nature remains neutral with regard to jurisdictional claims in published maps and institutional affiliations.